Nuclear Materials and Energy 19 (2019) 218–224

Contents lists available at ScienceDirect

Nuclear Materials and Energy

journal homepage: www.elsevier.com/locate/nme

Deposition of impurity metals during campaigns with the JET ITER-like Wall

A. Widdowson[a,*], J.P. Coad[a], E. Alves[b], A. Baron-Wiechec[a], N. Catarino[b], V. Corregidor[b], K. Heinola[c,d], S. Krat[e], C. Makepeace[f,a], G.F. Matthews[a], M. Mayer[g], K. Mizohata[d], M. Sertoli[g], JET Contributors[1], EUROfusion Consortium, JET, Culham Science Centre, Abingdon, OX14 3DB, UK

[a] Culham Centre for Fusion Energy, Culham Science Centre, Abingdon, OX14 3DB, UK
[b] Instituto Superior Técnico, Universidade de Lisboa, 1049-001 Lisboa, Portugal
[c] International Atomic Energy Agency, Vienna International Centre, P.O. Box 100, 1400 Vienna, Austria
[d] University of Helsinki, P.O. Box 64, 00560 Helsinki, Finland
[e] National Research Nuclear University MEPhI, Moscow, Russia
[f] Department of Materials, University of Oxford, Parks Road, Oxford OX1 3PH, UK
[g] Max-Planck-Institut für Plasmaphysik, 85748 Garching, Germany

ARTICLE INFO

Keywords:
JET
Erosion
Deposition
Impurities
Nickel
Tungsten

ABSTRACT

Post mortem analysis shows that mid and high atomic number metallic impurities are present in deposits on JET plasma facing components with the highest amount of Ni and W, and therefore the largest sink, being found at the top of the inner divertor. Sources are defined as “continuous” or “specific”, in that “continuous” sources arise from ongoing erosion from plasma facing surfaces and “specific” are linked with specific events which decrease over time until they no longer act as a source. This contribution evaluates the sinks and estimates sources, and the balance gives an indication of the dominating processes. Charge exchange neutral erosion is found to be the main source of nickel, whereas erosion of divertor plasma facing components is the main source of tungsten. Specific sources are shown to have little influence over the global mid- and high-Z impurity concentrations in deposits.

1. Introduction

After three operating campaigns of JET with the ITER-like Wall (JET-ILW) the evolving picture of fuel retention [1,2] and material migration [3] has been well documented. The effect of the campaign average plasma configurations on the global erosion of plasma facing components (PFCs), migration of eroded material and eventual deposition are largely understood [4]. Erosion from plasma interaction may occur as a result of several processes: (i) during limiter plasmas - erosion of limiters where direct contact between plasma and PFCs occurs [5], (ii) during divertor plasmas - erosion of divertor surfaces due to sputtering by incoming energetic ions at or near the strike point positions, and (iii) for all phases - charge exchange neutrals (CXN) coming from the plasma that can erode all surfaces, including those that are recessed from the plasma, i.e., that do not experience direct plasma contact. The erosion processes (i) and (iii) occur in the main chamber and provide a source of impurities which can enter the plasma or the scrape off layer (SOL). Impurities in the SOL migrate around the edge of the plasma primarily to the inner divertor surfaces during divertor plasmas giving rise to deposition. Most deposition occurs at the upper inner divertor as this is accessible from the SOL for all plasma configurations, however more complicated patterns of deposition arise due to variations in the location of the strike point positions. Deposition can also occur in the main chamber mainly during limiter plasmas, for example at the ends of limiter tiles that are located deep into the SOL. For JET the main impurities in the deposits are beryllium (Be) eroded from the main chamber limiters, carbon (C), a residual in the machine coming from remote components, and oxygen (O) due to uncontrolled sources of oxygen such as water, oxides on tiles and a low-level air leak. Deuterium (D) is the principal plasma fuel, some of which is co-deposited with the Be and C. Mid-atomic number (Z) and high-Z metals are also found in deposits. The presence of tungsten (W) and molybdenum (Mo) in deposits is not surprising as all divertor PFCs and some recessed main chamber PFCs have a W surface, either as bulk material or as a coating on a carbon fibre composite (CFC) substrate with a Mo interlayer and W top layer. Mid-Z impurities such as nickel (Ni), chromium (Cr) and iron (Fe) are also abundant in JET as the vessel's structural components are made of nickel alloys such as Inconel.

* Corresponding author.
E-mail address: anna.widdowson@ukaea.uk (A. Widdowson).
[1] See the author list of X. Litaudon et al 2017 Nucl. Fusion 57 102001.

https://doi.org/10.1016/j.nme.2018.12.024
Received 31 July 2018; Received in revised form 19 December 2018; Accepted 20 December 2018

This manuscript reports on the mid- and high-Z impurities found in JET PFCs and the magnitudes of the potential sources are discussed. The evaluation has assisted in determining which processes are the dominant sources. It is found that continuous sources, i.e., those that continue throughout the operating period, are the largest sources. The main continuous sources are from W erosion in the divertor and charge exchange neutral (CXN) erosion of Ni, Fe and Cr in the main chamber. In contrast, specific sources from one-off events may give rise to an increased source for a short period of time. Eventually, however, the liberated material migrates to remote areas where no further plasma interaction occurs. In future tokamaks this will mean that one-off events giving rise to unwanted impurities will eventually dissipate.

2. Experimental details

After each JET operating period a set of PFCs (tiles) and other components are removed for analysis to understand surface erosion, deposition and fuel retention. JET-ILW has now completed three periods of operation; 2011–12 (ILW1), 2013–14 (ILW2) and 2015–16 (ILW3) and analysis of tiles allows comparison between these periods. This manuscript does not provide the details of erosion and deposition of the major Be impurity and co-deposition of D, C and O; it reports primarily on W, Ni, Cr and Fe impurities. Deposits are principally characterised using ion beam analysis (IBA) techniques such as nuclear reaction analysis (NRA), back scattering of proton beam (PBS) and particle induced x-ray emission (PIXE). Details of the techniques are given in [3] and [6]. The overall concentrations of the mid- and high-Z impurities follow the deposition patterns of Be, D, C, O. In the following sections the results presented on the W divertor tiles are mainly for Ni, Cr, Fe due to the difficulty in accurately determining W in deposits on a W substrate. However, diagnostics located in the divertor corners were made of either steel (a grade with no W) or Ni-based alloys, so W analysis was possible. The Be main chamber tiles analysed after ILW1 and ILW2 were marker tiles designed to measure erosion/deposition by coating with an interlayer of Ni (~3 μm) and a top coat (~7 μm) of Be. This makes analysis of Ni deposition difficult, so the results presented for these campaigns are only for W. Tiles exposed during ILW3 did not have the marker coatings, thus facilitating analysis of both Ni and W.

3. Results and discussion

3.1. Mid- and high-atomic number metal impurities in the divertor

3.1.1. Mid-atomic number impurities in the divertor

Beryllium eroded from the main chamber has been shown previously to be mostly deposited at the top of the inner divertor on Tile 1 and the High Field Gap Closure (HFGC) tile [1,3,6,7]. The Be deposition on Tile 1 was restricted to the upper part of the tile during ILW1 (s-coordinate 162–280 mm – see inset in Fig. 1) but extended over the rest of the tile for ILW2 due to the use of a wider range of strike point positions [4]. Fig. 1 shows that the situation is the same for Ni, and the profile for the tile exposed for ILW3 only is similar to that exposed for ILW2 only. The amounts of Ni averaged over Tile 1 for ILW1, 2 and 3 are 1.4, 1.8 and 2.4% of the corresponding amounts of Be (respectively). The Cr and Fe concentrations follow the same pattern as the Ni but are each smaller by a factor 3–4. This agrees with the relative concentrations in Inconel (Ni 50–80%, Cr ~20%, Fe 5–20% depending on grade) and points to Inconel as the source of these impurities (see also Section 3.3.). Extrapolating the Ni deposition at the upper inner divertor Tile 1 for the whole divertor, assuming toroidal symmetry for ninety-six identical Tile 1 s, gives a total deposition of the order 10^{22} Ni atoms for a campaign consisting of $\sim 5 \times 10^4$ s of plasma.

As for Tile 1, mid-Z impurities are found in all deposits in the divertor. For example, the re-deposition bands on inner divertor corner Tile 4 and outer divertor corner Tile 6 [2,4,6,8] also contain Ni, Cr and Fe. For Tile 6 the amount of deposition increases by an order of magnitude in this deposition band from $\sim 5 \times 10^{18}$ Be at/cm^2 for ILW1 to $\sim 4 \times 10^{19}$ Be at/cm^2 for ILW2 [4]. The overall increase in deposition is attributed to the increased time for the outer strike point (OSP) on Tile 6 of 2.8×10^4 s in ILW2 compared with 1.0×10^4 s in ILW1 [8]. However, analysis using PIXE shows a larger increase in mid-Z metals, thereby suggesting a higher concentration of Ni in the deposit after ILW2. The differences in the Ni concentrations on Tile 6 between ILW1 and ILW2 operations may be due to the melting of three tile tie rods at the outer divertor which occurred during ILW2 providing an additional source of Ni, Cr and Fe. This is discussed further in Section 3.3.

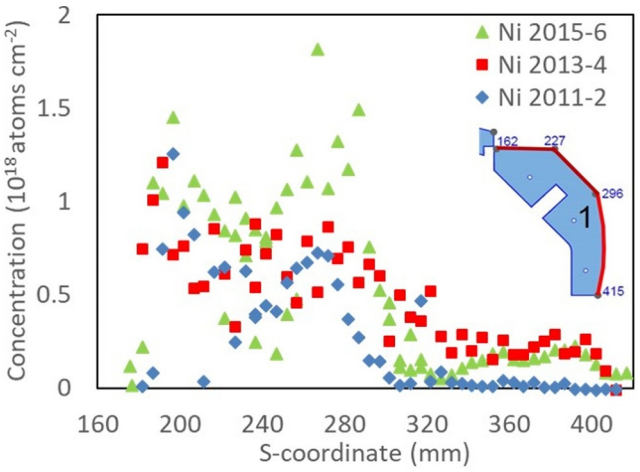

Fig. 1. Nickel concentrations across Tile 1 exposed for each of ILW1, ILW2 and ILW3. The total Ni concentration with respect to Be increased between operating period: 1.4% (ILW1), 1.8% (ILW2) and 2.4% (ILW3). Inset: cross-section of Tile 1 showing the s-coordinates along its surface.

Moon et al [9] compare deposits on molybdenum mirror samples exposed to ILW3 with those exposed for the three campaigns (ILW1-3). At the inner corner and base locations the impurity concentrations on the mirrors were 2–3 times greater following the three campaigns than after just ILW3. However, at the outer corner deposition was much more even when comparing ILW1-3 with ILW3. For Ni the levels were of the order 20×10^{15} at/cm^2, 1–2 orders of magnitude less than Be deposition. The difference in Ni levels for mirrors exposed for ILW3 only did appear to be rather closer to the ILW1-3 level than for other impurities, which may indicate an anomalous source of Ni at the outer corner.

3.1.2. Tungsten impurities in the divertor

All the PFC surfaces in the divertor are W - either as bulk W (Tile 5) or as thick W coatings (all other PFCs). On all these surfaces it is not possible to prove unambiguously whether W seen in the surface ion beam analysis (IBA) spectra is from deposition or from the W substrate. However, there are a number of diagnostics at the divertor corners shadowed from direct plasma bombardment that are not made from W such as louvre clips, mirrors, rotating collectors and Quartz Microbalances [10] on which W deposition can be measured. As an example, Fig. 2 shows W analysis data from a louvre clip at the outer divertor corner exposed to ILW2. The W level is in the range 2–10% of the Be concentration on the clip, which is typical for the many diagnostic components analysed (including those reported in [9,11]), and suggests that the total W deposition in the divertor corners during one ILW campaign is in the range 10^{20}–10^{21} atoms. However, it should be borne in mind that the majority of the (Be) deposition occurs at the top of the inner divertor, including 10^{20} at/cm^2 Be over a poloidal distance of >10 cm [3]. This equates to $\sim 10^{24}$ Be atoms toroidally, and if W is at 2% (similar to Ni) throughout these deposits then $\sim 2 \times 10^{22}$ atoms W would be included. The remote location of the louvre clip may indicate that migration of W is by line of sight transport due to erosion of

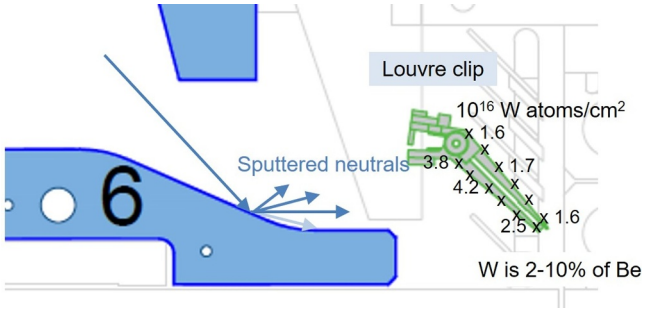

Fig. 2. Tungsten concentration on a louvre clip at the outer divertor corner exposed in ILW2.

W coatings when the strike point is on Tile 6 [12,13]. However, the end of the louvre clip blade has no direct line of sight from Tile 6, therefore migration must be multi-step which could involve: (i) reflections, i.e., low sticking coefficient, (ii) erosion of deposited W by sufficiently high energy neutrals for sputtering, (iii) high sputtering yield of W deposits or (iv) transport of W via formation of volatiles, e.g., oxides. Further modelling is required to understand the relative impact of these processes.

3.2. Mid- and high-atomic number metal impurities in the main chamber

3.2.1. Mid-atomic number impurities

The inner wall of the JET vessel has 16 poloidal Inner Wall Guard Limiter beams (IWGL), each of which is 320 mm wide. Ten of the IWGL beams are made up of bulk Be tiles. The other beams are made up of either W-coated CFC or Be-coated Inconel tiles and are recessed at least 25 mm behind the Be limiters. The gaps between the limiters are covered with either Be-coated Inconel tiles (69%) or W-coated CFC tiles (31%) recessed 40 mm behind the Be limiters; a schematic diagram is shown in [14].

Analysis shows that Ni, Cr and Fe are present in deposits on the Be limiter tiles. However the presence of the Ni based marker coatings on the tiles exposed during ILW1 and ILW2 (see Section 2) make it difficult to quantify Ni concentrations in the deposits. Therefore only data for the tile from ILW3 can be used to assess Ni concentration in deposits. Fig. 3(a) shows the Ni, Cr and Fe concentrations across a Be IWGL tile from the mid-plane that was exposed just during ILW3. The plasma is in contact with the central region of this tile during the limiter phases of each discharge (i.e. ramp-up and ramp-down), and the area is one of net erosion (by up to 60 μm during ILW1 [12]). Towards the toroidal ends of the limiter, the surfaces are progressively deeper into the SOL due to the curvature of the tile, and the region changes from net erosion to net deposition. The very ends of the tiles are shadowed by the next limiter in the poloidal direction, so the deposition there is reduced. The distribution of metals on the mid-plane IWGL reflects this description where concentration is low in the central region of the tile and peaked towards the ends. Cr and Fe are also seen along with W in cross section transmission electron micrographs of deposits on Be limiter tiles from ILW1, an example for Cr is also shown in Fig. 3(b). Fig. 3(a) clearly indicates that the relative concentrations of Ni, Cr and Fe in the deposit are the same as for Inconel alloys.

3.2.2. Tungsten impurities in the main chamber

Fig. 4 shows the W concentrations found on IWGL tiles exposed at the same mid-plane position for each of the ILW campaigns. As for Ni, Cr and Fe the W levels are low in the eroded central region. For ILW2 and ILW3 the W concentration decreases at the very ends of the tile (± 160 mm) due to the shadowing by the next limiter, however for ILW1 it increases to the very ends. This is likely due to an additional source of W in the main chamber during ILW1 which is discussed in Section 3.3.

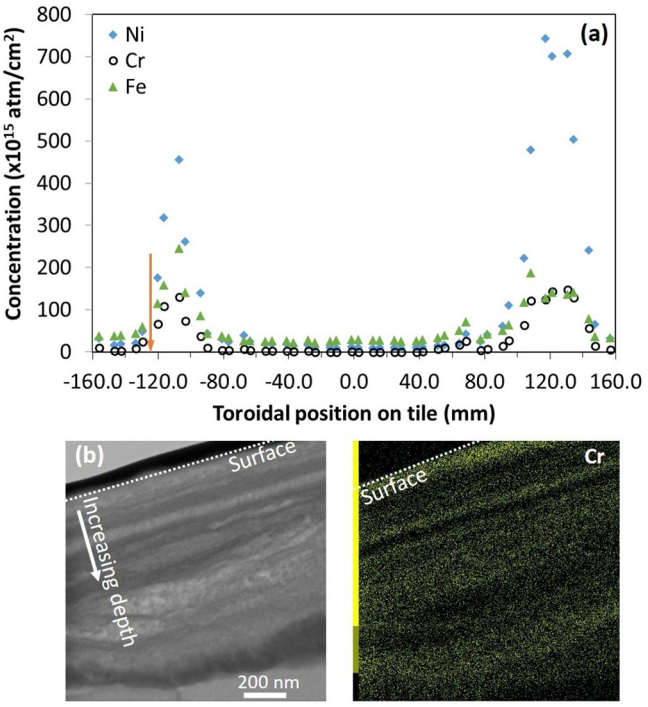

Fig. 3. (a) Nickel, chromium and iron concentrations on mid-plane inner wall guard limiter tile after ILW3. (b) Transmission electron micrograph and elemental analysis showing layered deposit containing chromium from ILW1 Be limiter tile. The arrow in (a) indicates the toroidal location of the micrographs. Also indicated by a cross in Fig. 4.

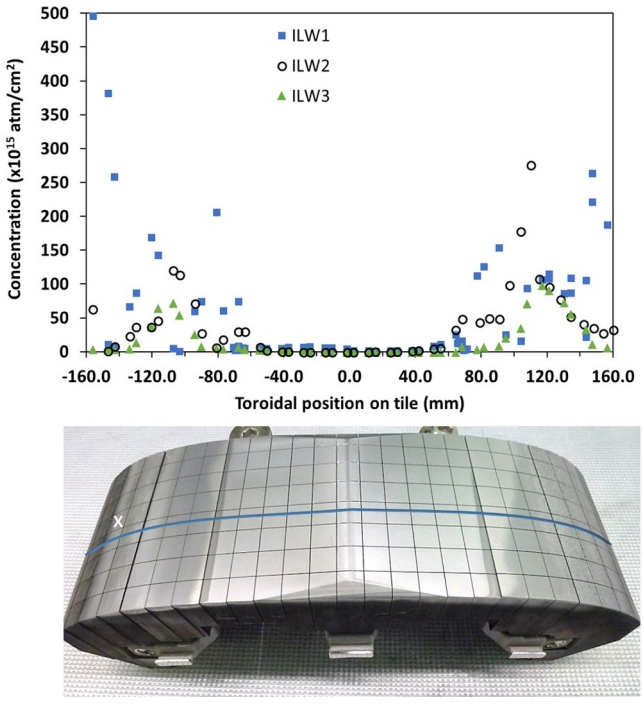

Fig. 4. Tungsten concentration on tiles located at the mid-plane of the IWGL after each ILW campaign. The line on the tile photograph indicates the analysis line toroidally across the tile. The cross on the left of the tile photograph indicates the location of the micrographs shown in Fig. 3.

Limiter tiles from the top and near the bottom of the limiter were also analysed after each ILW campaign. These tiles do not show erosion in their central region because in general limiter plasmas, which have a small radius compared with the limiter curvature, are not in direct

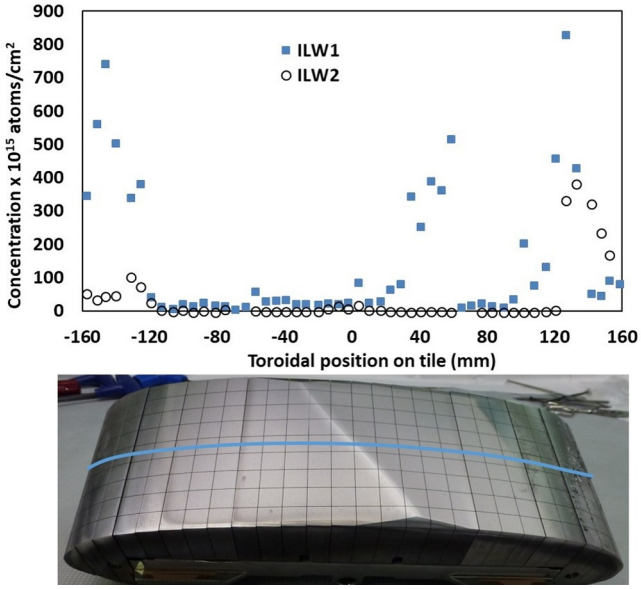

Fig. 5. Tungsten concentration on Be tiles located at mid-plane outer limiter after ILW1 and ILW2. The line on the tile photograph indicates the analysis line toroidally across the tile.

contact with the ends of the limiter beams for any significant time. Nor do the top and bottom tiles show such clear W peaks at the edges of the tiles after ILW1.

There are also Be limiters protecting the outer wall and the many diagnostics and heating systems located there. Selected tiles from one of the Be Wide Poloidal Limiters (WPL) are also analysed after exposure to each campaign, these comprise seven tile segments toroidally as seen in Fig. 5. The W deposition on the mid-plane tile is also classic in behaviour with erosion of a few microns in the central region (for ~100 mm on either side of the tangency point for limiter discharges) and deposition peaking deeper into the SOL, as shown in Fig. 5. Fig. 5 does show one anomaly from this pattern: there is increased deposition to the right-hand side of the central tile exposed to ILW1 with a cut-off at the edge of this piece at the toroidal position on the tile = 60 mm. This is probably due to a larger misalignment between the central Be segment and the piece to its right, creating a larger shadowed area on the right-hand side of the central segment where material is deposited. Extrapolating for IWGL and WPL tiles, the deposition of W on limiter tiles is ~ 10^{21} atoms for a campaign.

Figs. 3 and 4 show that Ni concentrations are a factor 2–3 times higher than for W on the mid-plane IWGL, which indicates a higher source of Ni relative to W reaching the main chamber. The analysis of the W and Ni sources potentially reaching the main chamber are discussed in Section 3.3 and are a similar order of magnitude. It is not possible to determine the concentration relative to Be from IBA data due to the Be substrate.

3.3. Sources of mid- and high-atomic number impurities

There are two categories of sources of mid-Z and high-Z impurities to consider: sources that are on-going during plasma operations, "continuous sources" and sources that exist for a limited time, "specific sources". In both cases the impurities migrate through multi-step erosion/deposition processes until they reach a surface where they can no longer be re-eroded. A continuous source, however, will result in a continual build-up of impurities on remote surfaces whereas a specific source will decrease with time. In this section examples of continuous and specific sources for both mid- and high-Z impurities are presented and where possible their relative magnitude evaluated.

3.3.1. Continuous sources

All divertor PFCs and some recessed main chamber PFCs have a W surface, either as bulk material or as a coating on a CFC substrate with a Mo interlayer and W top layer. Therefore, there is a significant source of W due to sputtering at these surfaces. W erosion is dominated by sputtering at the strike point on divertor PFCs, but other contributions include CXN erosion of W coated surfaces at the inner wall and sputtering on divertor PFCs wetted by field lines from ICRF heating [15], these latter two mechanisms and potential sources are discussed later in this section. W erosion of divertor PFCs is measured as ~ 1.5 μm (~10^{19} at/cm^2) for ILW2 on Tile 5 and Tile 6 where the strike point was located [7]. Taking a conservative total erosion area of 10.8 × 10^3 cm^2, i.e., two regions extending 5 cm poloidally on Tile 5 and Tile 6 for ILW2 (see [7]) and accounting for shadowing between tiles reducing the overall area, this constitutes a potential net W source up to 10^{23} atoms, which is considerably higher than the 10^{20}–10^{21} atoms that are found to migrate to the remote corners. However, as mentioned in Section 3.2.2, if W is ~2% of the deposited Be elsewhere in the divertor, ~2 × 10^{22} W atoms may be in deposits at the top of the inner divertor. Furthermore, some of the eroded W will be deposited locally either within the gaps between lamellae of Tile 5 or in the deposition peak at the bottom of the sloping part of Tile 6. Nevertheless, not all of the eroded material has been accounted for in the *post mortem* analysis of the divertor deposits and it would appear that a large fraction of the W eroded from Tile 5 and 6 must enter the plasma and migrate to the main chamber.

The JET vessel is manufactured mainly from Inconel® 600. Support brackets, fastenings and in-vessel furniture are also made from Inconel, or similar Ni-based alloys. Therefore, despite all surfaces with direct interaction with the confined plasma and all the inner wall PFCs being made of either Be or W, 85.4 m^2, or >60% of the main chamber surface at the top and outer vessel walls is unclad Inconel and is exposed to CXNs exiting the plasma. CXNs can have sufficient energy to sputter elements from these surfaces (mostly Ni, Cr and Fe), and this is assumed to be the reason why these elements have always been observed in the JET plasma and also found in deposits on PFCs [16].

Indeed erosion of the recessed surfaces of the JET vessel wall by CXNs has been measured throughout JET operations using C, Be and W coatings on samples inserted into inner wall cladding tiles [14] [17]. The most recent analysis for JET-ILW shows erosion rates of 0.6 × 10^{14} at/cm^{2}s and 9.2 × 10^{11} at/cm^{2}s for Be and W respectively [14]. From these erosion rates the ratio of the W and Be sputtering yields Y_W/Y_{Be} is 0.015. Taking empirical equations for sputter yield for W, Be and Ni [18,19], the energy at which Y_W/Y_{Be} = 0.015 is 635 eV. Assuming mono-energetic CXN particles at this energy would give a yield for Ni of 3.7 × 10^{13} at/cm^{2}s. A more detailed calculation using a Maxwellian CXN energy distribution might give a slightly different Ni erosion rate, but the resulting Ni source is likely to be in the range 10^{23}–10^{24} atoms during a campaign lasting of the order 5 × 10^4 s. Even if parts of the vacuum vessel are coated with impurities (e.g., C, Be) from previous operations, these figures suggest that CXN erosion may be the largest source of mid-Z impurities in the main chamber and can account for the 10^{22} atoms of Ni estimated to be in deposits, see Section 3.1.1.

An increased W content is observed in ICRF heated plasmas in the JET-ILW [20]. The source of the W is likely from regions where field line connections between the ICRF antennas and the divertor occur giving rise to physical sputtering of W by Be ions. Wetted areas include the top of the inner divertor and outer divertor [15]. The top of the outer divertor is a net erosion zone and can be a source of W. Erosion of just 0.01–0.1 μm of W from this area could provide a source of 10^{21}–10^{22} W atoms over a campaign. At the top of the inner divertor (Tile 1 and High Field Gap Closure tiles further inboard) the PFCs are covered by Be deposits. Therefore, at these surfaces erosion will be of mainly Be deposits (and not pure W) that contain Ni at a concentration of 10^{18} at/cm^2 and W (likely to be at a similar concentration although

not directly quantified for Tile 1). Other field line connections to the inner and outer main chamber wall may also promote re-erosion of deposits that have formed on limiters. In this respect the interaction with deposits arising from ICRF operations may serve to re-erode and re-distribute mid- and high-Z impurities that have originated from other sources. The ICRF antenna itself could also act as a source of Ni. Whilst much of the antennae is surrounded by Be tiles and components, there remain some Inconel components, “knuckles”, which could increase the Ni source. However, this source does not need to be invoked to balance the Ni sources and sinks, since CXN erosion in the main chamber from 10% of the unclad Inconel vessel wall (10^{22}–10^{23} as discussed in Section 3.3.1) can already provide for the divertor deposition sink of 10^{22} Ni atoms (as discussed in Section 3.2.1). Nevertheless, a further spectroscopic study of the levels of Ni in the plasma would assist in confirming which sources are significant.

3.3.2. Specific sources

A source of mid-Z impurities in the JET plasma was suspected to be due to the failure of three tile tie rods during ILW2. Tie rods made of Inconel® 718 are inserted into the CFC substrate of divertor tiles to prevent tiles from breaking apart in the event of cracking between fibre planes. When the vessel was vented and an in vessel photographic survey undertaken, three broken tie rods that were mounted in a vertical position in Tile position 7 were found partially melted in the outer divertor gap leading to the pumps (one in each of octants 1, 6 and 7). As impurities in deposits build up primarily due to material migration from the SOL, it follows that impurity concentrations in deposits might reflect plasma concentrations. However there is an increase in Ni with respect to Be in deposits on Tile 6 s between ILW1 and ILW2 (as discussed in Section 3.1) which may therefore be due to the tie rod melting.

There is no conclusive evidence that the tie rod melting resulted in an increase in Ni in the plasma beyond the outer divertor corner. From *post mortem* analysis there are no significant differences in the amounts of Ni in deposits on main chamber Be tiles and so far, analysis of the VUV spectroscopy of Ni, Cr or Fe cannot be linked consistently with any specific period when each tie rod may have failed and started to melt (or a general increase once melting was ongoing) with *outer corner* plasma configurations.

Another metric for analysis of impurities is to consider transient impurity events (TIE), i.e., excursions in optical spectroscopy signals due to particles entering the plasma. The number of TIEs for W and Ni/Cr/Fe are plotted for characteristic spectral lines for each category against the pulse number during each campaign, as described in [21] and shown in Fig. 6. It is clear that there is a steady decline in the average number of events from ILW1 to ILW2 to ILW3. There is also a peak in the early discharges for the ILW1 and ILW2 campaigns, which may result from dust and debris caused by in-vessel work and installation of new components during the preceding shut-down. For example, W particles could be ejected during plasma operation from coating asperities and imperfections on new tiles installed for ILW1, or Ni, Cr, Fe debris could remain in vessel after installation work involving cutting, welding and grinding at the vessel wall after ILW1 and ILW2 which would decrease over time. Notably, no significant increase in TIE for Ni, Cr, Fe was observed during ILW2 that might be correlated with the tie rod failures mentioned above, as might be expected if molten material was ejected from this location.

Many of the W transients observed may be ascribed to small particles of W coating entering the plasma and such particles have been observed by visible and infrared camera viewing systems being ejected from the divertor region [22]. In addition small W particles were observed by TEM in deposits following ILW1 [23].

W coatings were also found to undergo cracking and delamination due to expansion mis-match in one direction between the coating and substrate as a result of rapid thermal cycling due to plasma interaction (which can be between 200 and 1000 °C). This was particularly evident

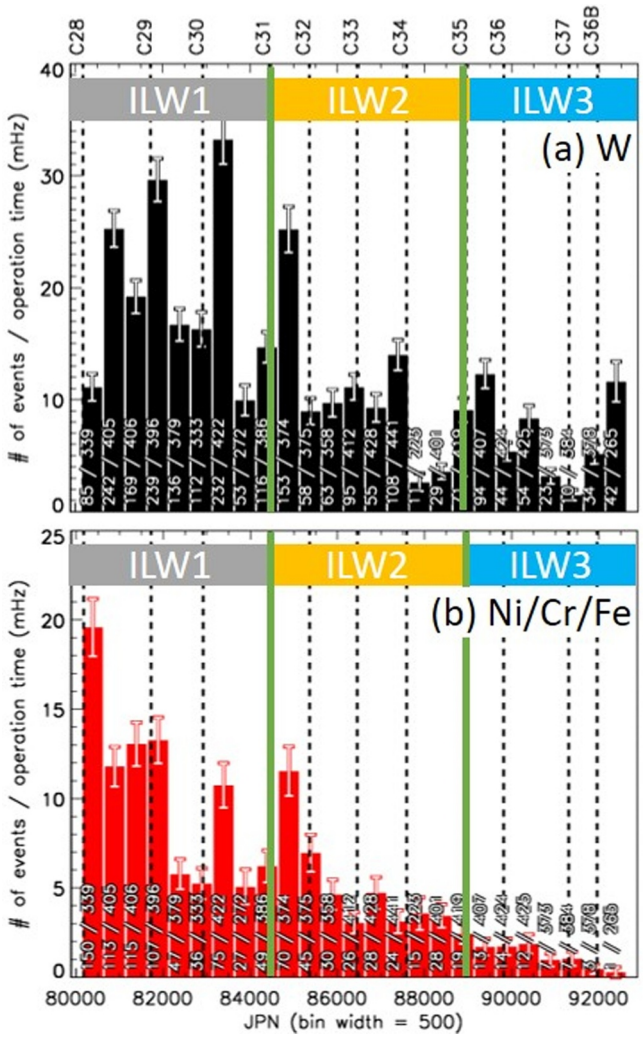

Fig. 6. Transient impurity events for ILW1, ILW2 and ILW3 for (a) tungsten and (b) nickel, chromium iron particles. For each bar the number of TIEs for the given element(s) and total number of TIEs per 500 pulse bin width are shown.

for divertor Tile 6 s and Tile7s during ILW1 and ILW2 where some tiles were prone to coating failure due to a process issue for a specific coating batch. Therefore, between ILW2 and ILW3 operations some of these tiles were replaced. In total six out of forty-eight Tile 7 s and twelve out of ninety-six Tile 6 s were replaced, of which a total of eight removed were from the defective batch. Other reasons for replacements were due to cracking of tiles, large molten splats, design modifications or retrieval for *post mortem* analysis. Analysis of W TIEs suggests that the source is 10^{21} W atoms [21] whereas an estimate of cracking/delamination area from divertor PFCs could yield up to 10^{23} W atoms. This suggests that only a small percentage of particles travel to the plasma. There is evidence that suggests thermal cracking of coatings is associated with melting and formation of small spheres alongside the cracks rather than ejection of particles. An example is shown in Fig. 7. In addition tungsten particles encapsulated by deposits have been observed [8]. The analysis also shows that overall TIEs constitute a specific source decreasing with operating time which is inconsistent with our understanding of time evolution of W coating cracking issues in JET.

In the shutdown after ILW1 the W coating on some tiles alongside the channel for the neutral beam entering the vessel from the mid-plane of Octant 8 and Octant 4 were found to have been eroded [12]. The area of coating eroded was ~100 cm^2, which equates to 10^{22} W atoms; there does not appear to have been significant further erosion during ILW2

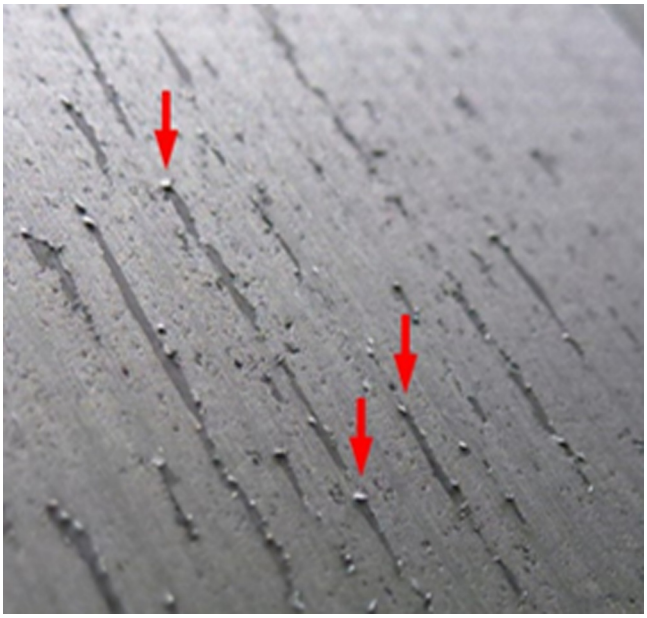

Fig. 7. Photograph showing delamination of W coating on outer divertor tile. Delaminations run along the direction of CFC laminations. Delaminated material tends to form into spheres at the edges of the delaminated region. Some examples are indicated by arrows.

and 3. This W may have contributed to the general level of W deposition during ILW1 and constitutes a specific source and may explain the increased level of W on the ends of the ILW1 mid-plane IWGL (Fig. 4). Some of the TIE may well have been triggered by this coating erosion.

4. Summary

The sources and sinks for mid- and high-Z impurities found from *post mortem* analysis help to inform the erosion processes dominating their production. Although the Ni concentration on the IWGL for ILW3 is slightly higher than the W concentration, they are essentially of the same order of magnitude, thus indicating that the sources are of similar magnitude. The main candidate for erosion of Ni is the CXN erosion of the recessed main vessel chamber and is potentially of the order 10^{23}–10^{24} atoms per campaign. However, the vessel wall may be coated with impurities which could reduce the source. This would result in a decrease in the Ni source to $\sim 10^{22}$ atoms per campaign. For W there are three possible sources: (i) erosion from the outer divertor at 10^{23} atoms per campaign, (ii) erosion by ions following field line connections at the top of the outer divertor, which could provide 10^{21}–10^{22} atoms for 0.01–0.1 μm net erosion and (iii) particles from coating imperfections and fatigue cracking creating TIEs, estimated as a source of 10^{21} atoms per campaign. Of these three sources, erosion from the outer divertor provides the main W source. The contribution from TIEs is found to be low, indicating that dust is not a major contributor of impurities in the plasma.

Overall, specific sources do not have a significant bearing as they decrease over time and eventually the source material migrates to remote surfaces. The melted tie rods were perceived as affecting plasma operations, but the increase in Ni concentration on Tile 6 shown in *post mortem* analysis is probably only a local effect as no consistent correlation with Ni concentration in the plasma from VUV and TIE measurements has been established with *outer corner* plasma configurations.

The main sink for impurities is the top of Tile 1 at the inner divertor, where the most deposition and fuel retention occurs. The sink is estimated at 10^{22} Ni atoms per campaign (and although it cannot be quantified by IBA, is probably of a similar magnitude for W). In terms of mid- and high-Z material balance this is consistent with the dominant source mechanisms identified which are $\sim 10^{22}$ atoms for Ni and 10^{22}–10^{23} for W. The comparison of the Ni sources and sinks indicates that there is no need to invoke a source originating from the ICRH antennae to achieve a material balance.

The presentation of the material balance for mid- and high-Z impurity sources and sinks has highlighted some areas for further work, for example, the evaluation of Ni and W in the plasma from spectroscopy signals to compare with the magnitude of the erosion sources ascertained here. In addition, an assessment of CXN neutral erosion of the vessel wall could provide insight for the evaluation of material lifetime of future devices. It is also necessary to continue the reporting of W and Ni, Cr, Fe data from *post mortem* analysis as these impurities have acted as markers which have facilitated in the identification of the erosion dominant sources. The results provide useful benchmarking data for modelling. For example, the assessment of CXN erosion rates, particularly for W and Be that have been measured at the inner wall and the potential Ni erosion source estimated here. Also the local and long-range migration data for mid- and high-Z impurities, in comparison with Be, could be used to validate SOL transport and local erosion/deposition effects.

Conflict of interest

The authors declare that they have no known competing financial interests or personal relationships that could have appeared to influence the work reported in this paper.

Acknowledgements

This work has been carried out within the framework of the EUROfusion. Consortium and has received funding from the Euratom research and training programme 2014-2018 under grant agreement no. 633053 and from the RCUK Energy Programme [grant number EP/I501045]. To obtain further information on the data and models underlying this paper please contact PublicationsManager@ccfe.ac.uk. The views and opinions expressed herein do not necessarily reflect those of the European Commission.

Supplementary material

Supplementary material associated with this article can be found, in the online version, at doi:10.1016/j.nme.2018.12.024.

References

[1] K. Heinola, A. Widdowson, J. Likonen, E. Alves, A. Baron-Wiechec, N. Barradas, S. Brezinsek, N. Catarino, P. Coad, S. Koivuranta, G.F. Matthews, M. Mayer, P. PeterssonJET-EFDA Contributors, Fuel retention in JET ITER-Like Wall from post-mortem analysis, J. Nucl. Mater. 463 (2015) 961–965, https://doi.org/10.1016/j.jnucmat.2014.12.098.

[2] K. Heinola, A. Widdowson, J. Likonen, T. Ahlgren, E. Alves, C.F. Ayres, A. Baron-Wiechec, N. Barradas, S. Brezinsek, N. Catarino, P. Coad, C. Guillemaut, I. Jepu, S. Krat, A. Lahtinen, G.F. Matthews, M. MayerJET Contributors, Experience on divertor fuel retention after two ITER-Like Wall campaigns, Phys. Scr. T170 (2017) 014063http://iopscience.iop.org/article/10.1088/1402-4896/aa9283/meta.

[3] M. Mayer, S. Krat, W. Van Renterghem, A. Baron-Wiechec, S. Brezinsek, I. Bykov, P. Coad, Y. Gasparyan, K. Heinola, J. Likonen, A. Pisarev, C. Ruset, G. de Saint-Aubin, A. WiddowsonJET Contributors, Erosion and deposition in the JET divertor during the first ILW campaign, Phys. Scr. T167 (2016) 014051, , https://doi.org/10.1088/0031-8949/T167/1/014051.

[4] A. Widdowson, J.P. Coad, E. Alves, A. Baron-Wiechec, N.P. Barradas, S. Brezinsek, N. Catarino, V. Corregidor, K. Heinola, S. Koivuranta, S. Krat, A. Lahtinen, J. Likonen, G.F. Matthews, M. Mayer, P. Petersson, M. RubelJET Contributors, Overview of fuel inventory in JET with the ITER-like wall, Nucl. Fusion. 57 (2017) 086045, , https://doi.org/10.1088/1741-4326/aa7475.

[5] A. Widdowson, E. Alves, C.F. Ayres, A. Baron-Wiechec, S. Brezinsek, N. Catarino, J.P. Coad, K. Heinola, J. Likonen, G.F. Matthews, M. Mayer, M. RubelJET-EFDA Contributors, Material migration patterns and overview of first surface analysis of the JET ITER-like wall, Phys. Scr. T159 (2014) 014010, , https://doi.org/10.1088/0031-8949/2014/T159/014010.

[6] N. Catarino, N.P. Barradas, V. Corregidor, A. Widdowson, A. Baron-Wiechec, J.P. Coad, K. Heinola, M. Rubel, E. Alves, JET Contributers, Assessment of erosion,

deposition and fuel retention in the JET-ILW divertor from ion beam analysis data, Nucl. Mater. Energy 12 (2017) 559–563, https://doi.org/10.1016/j.nme.2016.10.027.

[7] M. Mayer, S. Krat, A. Baron-Wiechec, Y. Gasparyan, K. Heinola, S. Koivuranta, J. Likonen, C. Ruset, G. De Saint-Aubin, A. WiddowsonJET Contributors, Erosion and deposition in the JET divertor during the second ITER-like wall campaign, Phys. Scr. (2017) 014058, , https://doi.org/10.1088/1402-4896/aa8ff9.

[8] A. Widdowson, E. Alves, A. Baron-Wiechec, N.P. Barradas, N. Catarino, J.P. Coad, V. Corregidor, A. Garcia-Carrasco, K. Heinola, S. Koivuranta, S. Krat, A. Lahtinen, J. Likonen, M. Mayer, P. Petersson, M. Rubel, S. Van Boxel, Overview of the JET ITER-like wall divertor, Nucl. Mater. Energy 12 (2017) 499–505, https://doi.org/10.1016/j.nme.2016.12.008.

[9] Sunwoo Moon, P. Petersson, M. Rubel, E. Fortuna-Zalesna, A. Widdowson, S. Jachmich, A. Baron-Wiechec, A. Litnovsky, E. AlvesJET Contributors, First Mirror Test in JET for ITER: complete overview after three ILW campaigns, Nucl. Mater. Energy 19 (2019) 59, https://doi.org/10.1016/j.nme.2019.02.009.

[10] J.P. Coad, H.-G. Esser, J. Likonen, M. Mayer, G. Neill, V. Philipps, M. Rubel, J. VinceJET-EFDA Contributors, Diagnostics for studying deposition and erosion processes in JET, Fusion Eng. Des. 74 (2005) 745–749, https://doi.org/10.1016/j.fusengdes.2005.06.217.

[11] P. Ström, P. Petersson, M. Rubel, E. Fortuna-Zaleśna, A. Widdowson, G. SergienkoJET Contributors, Analysis of deposited layers with deuterium and impurity elements on samples from the divertor of JET with ITER-like wall, J. Nucl. Mater. (2018), https://doi.org/10.1016/j.jnucmat.2018.11.027.

[12] A. Widdowson, J.P. Coad, E. Alves, A. Baron-Wiechec, N.P. Barradas, N. Catarino, V. Corregidor, K. Heinola, S. Krat, J. Likonen, G.F. Matthews, M. Mayer, P. Petersson, M. RubelJET Contributors, Impurity re-distribution in the corner regions of the JET divertor, Phys. Scr. T170 (2017) 014060, , https://doi.org/10.1088/1402-4896/aa90d5.

[13] A. Kirschner, S. Brezinsek, A. Huber, A. Meigs, G. Sergienko, D. Tskhakaya, D. Borodin, M. Groth, S. Jachmich, J. Romazanov, S. Wiesen, C. LinsmeierJET Contributors, Modelling of tungsten erosion and deposition in the divertor of JET-ILW in comparison to experimental findings, Nucl. Mater. Energy 18 (2019) 239–244, https://doi.org/10.1016/j.nme.2019.01.004.

[14] S. Krat, Y. Gasparyan, A. Pisarev, I. Bykov, M. Mayer, G. de Saint Aubin, M. Balden, C.P. Lungu, A. WiddowsonJET-EFDA contributors, Erosion at the inner wall of JET during the discharge campaign 2011–2012 in comparison with previous campaigns, J. Nucl. Mater. 456 (2015) 106–110, https://doi.org/10.1016/j.jnucmat.2014.08.010.

[15] V. Bobkov, D. Aguiam, R. Bilato, S. Brezinsek, L. Colas, A. Czarnecka, P. Dumortier, R. Dux, H. Faugel, H. Fünfgelder, P. Jacquet, A. Kallenbach, A. Krivska, C.C. Klepper, E. Lerche, Y. Lin, D. Milanesio, R. Maggiora, I. Monakhov, R. Neu, J.-M. Noterdaeme, R. Ochoukov, T. Pütterich, M. Reinke, W. Tierens, A. Tuccillo, O. Tudisco, D. Van Eester, J. Wright, S. Wukitch, W. Zhangthe ASDEX Upgrade Team, the Alcator C-Mod Team, the EUROfusion MST1 Team, JET Contributors, Impact of ICRF on the scrape-off layer and on plasma wall interactions: From present experiments to fusion reactor, Nucl. Mater. Energy 18 (2019) 131–140, https://doi.org/10.1016/j.nme.2018.11.017.

[16] J.P. Coad, J. Likonen, M. Rubel, E. Vainonen-Ahlgren, D.E. Hole, T. Sajavaara, T. Renvall, G.F. MatthewsJET EFDA Contributors, Overview of material re-deposition and fuel retention studies at JET with the Gas Box divertor, Nucl. Fusion 46 (2006) 350–366, https://doi.org/10.1088/0029-5515/46/2/018.

[17] M. Mayer, S. Krat, J.P. Coad, A. Hakola, J. Likonen, S. Lindig, A. WiddowsonJET-EFDA Contributors, Erosion at the inner wall of JET during the discharge campaigns 2001–2009, J. Nucl. Mater. 438 (2013) S780–S783, https://doi.org/10.1016/j.jnucmat.2013.01.167.

[18] M. Schmid, Sputter Yield Calculator, https://www.iap.tuwien.ac.at/www/surface/sputteryield, (2009).

[19] N. Matsunami, Y. Yamamura, Y. Itikawa, N. Itoh, Y. Kazumata, S. Miyagawa, K. Morita, R. Shimizu, H. Tawara, Energy dependence of the ion-induced sputtering yields of monatomic solids, At. Data Nucl. Data Tables. 31 (1984) 1–80, https://doi.org/10.1016/0092-640X(84)90016-0.

[20] V. Bobkov, G. Arnoux, S. Brezinsek, J.W. Coenen, L. Colas, M. Clever, A. Czarnecka, F. Braun, R. Dux, A. Huber, P. Jacquet, C. Klepper, E. Lerche, C. Maggi, F. Marcotte, M. Maslov, G. Matthews, M.L. Mayoral, K. McCormick, A. Meigs, D. Milanesio, I. Monakhov, R. Neu, J.-M. Noterdaeme, T. Pütterich, F. Rimini, G. Van Rooj, G. Sergienko, D. Van EesterJET EFDA Contributors, ICRF specific plasma wall interactions in JET with the ITER-like wall, J. Nucl. Mater. 438 (2013) S160–S165, https://doi.org/10.1016/J.JNUCMAT.2013.01.044.

[21] M. Sertoli, J.C. Flanagan, M. Bacharis, O. Kardaun, A. Jarvinen, G.F. Matthews, S. Brezinsek, D. Harting, A. Cackett, E. Hodille, I.H. Coffey, E. Lazzaro, T. PütterichJET Contributors, Impact of W events and dust on JET-ILW operation, J. Nucl. Mater. 463 (2015) 837–841, https://doi.org/10.1016/j.jnucmat.2014.12.033.

[22] J.C. Flanagan, M. Sertoli, M. Bacharis, G.F. Matthews, P.C. De Vries, A. Widdowson, I.H. Coffey, G. Arnoux, B. Sieglin, S. Brezinsek, J.W. Coenen, S. Marsen, T. Craciunescu, A. Murari, D. Harting, A. Cackett, E. HodilleJET-EFDA Contributors, Characterising dust in JET with the new ITER-like wall, Plasma Phys. Control. Fusion. (2015) 57, https://doi.org/10.1088/0741-3335/57/1/014037.

[23] M. Rubel, A. Widdowson, J. Grzonka, E. Fortuna-Zalesna, Sunwoo Moon, P. Petersson, N. Ashikawa, N. Asakura, D. Hamaguchi, Y. Hatano, K. Isobe, S. Masuzaki, H. Kurotaki, Y. Oya, M. Oyaidzu, M. Tokitani, Dust generation in tokamaks: Overview of beryllium and tungsten dust characterisation in JET with the ITER-like wall, Fusion Eng. Des. 136 (2018) 579–586, https://doi.org/10.1016/j.fusengdes.2018.03.027.